Pergamon

0301-9322(94)00087-5

Int. J. Multiphase Flow Vol. 21, No. 3, pp. 419–436, 1995
Elsevier Science Ltd. Printed in Great Britain

EXPERIMENTAL STUDIES OF FLOODING IN NEARLY HORIZONTAL PIPES

KI YONG CHOI and HEE CHEON NO

Department of Nuclear Engineering, Korea Advanced Institute of Science and Technology, 373-1 Ku Song Dong, Yu Sung Gu, Taejon 305-701, Korea

(Received 22 September 1993; in revised form 22 November 1994)

Abstract—To investigate the flooding phenomenon in nearly horizontal pipes, experimental studies are performed for air and water countercurrent flow in a test section with a length of 2160 mm, with three different inner diameters of 40, 60 and 70 mm, with different types of end geometry, and with various inclination angles. The effects of the pipe diameter, end geometry and inclination angle on flooding are examined. Two mechanisms governing the transition to flooding are proposed: inner flooding and entrance flooding. The inner flooding is initiated by unstable wave growth, i.e. slugging, at the inner location of the pipe. The entrance flooding is always observed to take place at the entrance of the water flow without slugging. The effect of the inclination angle on flooding is predominant within quite a narrow range of inclination ($0° < \theta < 1°$). A small deviation of the inclination angle from the horizontal plane causes a large deviation of the required air flow rates for flooding. Two local void fractions are measured by parallel wire probes and a scale marked rule in two regions (sub- and super-critical regions). The local effects of the void fraction on slug formation models are investigated. It is found that the differences in the exponents of the void fraction terms of the existing slug formation models mainly result from the definition of the void fraction used. When the void fraction measured in the sub-critical region is used in the slug formation model, Mishima *et al.*'s model well predicts the trend of the present data. However, if the void fraction measured in the super-critical region is used, Taitel *et al.*'s model better predicts the present data.

Key Words: flooding, horizontal, two-phase flow, air–water

1. INTRODUCTION

In recent years, flooding in stratified flow has been of interest in conjunction with nuclear power plants. In particular, during a postulated small break loss-of-coolant accident (SB-LOCA) in pressurized water reactors, PWRs, the countercurrent flow limit (CCFL) of steam and cold water may take place in a horizontal pipe or nearly horizontal pipe when ECC water is supplied through the pipe, which is one of the important phenomena affecting the thermal–hydraulic behavior in relation to the safety analysis of the pressurized water reactor, PWR. Therefore, it is necessary to understand the mechanism of flooding in a stratified countercurrent gas–liquid flow. Systematic studies on this flow will provide important information for our understanding of the flooding phenomena. However, most of our studies on flooding in the past were focused on vertical and horizontal pipes with a small diameter of less than about 0.10 m. It has been reported that flooding in horizontal pipes occurs at much lower gas velocities than in vertical pipes. So understanding the flooding phenomenon in horizontal geometry can give more conservative results from the viewpoint of safety. Up to now, there still exists a lack of data in the literature concerning horizontal or near-horizontal countercurrent flow.

Lee & Bankoff (1983b) investigated the flooding phenomenon in rectangular ducts inclined at various angles ($\theta = 2.9$, 4.5 and 33.5°). An envelope theory, which was based on the hydrodynamic and energy equations for the onset of flooding in a condensing flow, was developed and found to agree very well with the data. They observed the formation of a water slug at the bottom just before the onset of flooding in nearly-horizontal countercurrent flow. They compared their data with the slug formation models proposed by several investigators (Kordyban & Ranov 1970; Wallis & Dobson 1973; Taitel & Dukler 1976; Gardner 1979; Mishima & Ishii 1980). Lee & Bankoff (1983b) found that the slug formation model in cocurrent horizontal flow could be successfully employed for the prediction of the onset of flooding in nearly horizontal countercurrent flow, although these models were based on quite different assumptions.

Barnea *et al.* (1986) investigated the inception of flooding in inclined pipes over the whole range of inclinations both experimentally and theoretically. They showed that, depending on the liquid entrance geometry and liquid and gas flow rates, flooding initiation could be observed to take place in two different ways, i.e. a local disturbance generated at the liquid entrance and disturbance waves somewhere along the pipe. It was found that the effect of inclination is quite complex, and the flow rates at which flooding occurs increase and then decrease as the inclination angles increase from horizontal to vertical. Their noteworthy results are that a small deviation from the horizontal or the vertical position has the most pronounced effect on the initiation of flooding. They also developed a model based on a film theory in which the interfacial shear is used as input to predict the flooding limits. The agreement between the theory and the experimental results was satisfactory in the range where the correlation for the interfacial shear is reasonably accurate.

For vertical-to-horizontal pipes, Siddiqui *et al.* (1986) performed several experiments and studied the effect of pipe diameter, bend radius of curvature, horizontal pipe length, entrance geometry and slight inclination of the horizontal leg on the flooding phenomenon. They found that flooding is caused by unstable wave formation (slugging) at the hydraulic jump which forms in the lower pipe limb close to the bend. As the air flow rate is increased the location of the hydraulic jump moves closer to the elbow, and eventually slugging occurs which brings about flooding. They observed that flooding in the elbow geometry occurs at gas flow rates much smaller than those needed to produce flooding in a vertical pipe with the same diameter and that flooding inception coincides with unstable wave formation (slugging) in the lower leg of the elbow, close to the bend. A marked effect on the flooding phenomenon, in particular, is detected in that for a slight upward inclination the air flow rate needed to cause flooding is greatly reduced, whereas for an equal downward inclination the contrary is seen. They also correlated their data in terms of local void fraction ϵ_G at the crest of the hydraulic jump, and the non-dimensional air superficial velocity j_G^* as follows:

$$j_G^* = 0.2\epsilon^{3/2}. \quad [1]$$

Ardron & Banerjee (1986) developed a theoretical model to predict the flooding limit in a pipe elbow of which the upper limb is vertical and the lower limb is horizontal or slightly inclined. Their model assumes that smooth stratified flow exists in the lower limb of the elbow, with a free outfall at the exit. The effect of the length-to-diameter ratio of the horizontal pipe on the flooding limit is included in this model. Flooding was assumed to coincide with slug formation just downstream of the bend where the liquid depth was the greatest. Their model predicted the experimental results by Siddiqui *et al.* (1986) quite well. However, for the case where the lower limb of the elbow is downwardly inclined, their model becomes invalid for $j_L^{*1/2} \geqslant 0.2$, when a transition to superficial flow is predicted.

Kawaji *et al.* (1991) also conducted experiments with vertical-to-inclined pipes containing elbows of varying angles. In vertical-to-horizontal pipes, the formation of a hydraulic jump downstream of the elbow was observed at low liquid flow rates ($j_L^{*1/2} < 0.4$), which caused flooding at much lower gas flow rates in comparison with the vertical pipe data. An increase in liquid flow rates ($0.4 < j_L^{*1/2} < 0.7$) caused a shift of the location of the hydraulic jump toward the horizontal pipe exit away from the elbow, and flooding occurred at the pipe exit due to slugging. At the highest liquid flow rates ($j_L^{*1/2} > 0.8$), they found that flooding occurred in the vertical section near the porous liquid entry rather than in the horizontal section. They also suggested that the flooding mechanism for intermediate to high liquid flow rates in vertical-to-downwardly-inclined pipes is due to the breakup of a turbulent jet-like liquid stream that forms at the elbow, and subsequent entrainment/carryover of droplets by the countercurrent gas stream.

However, the satisfactory physical mechanism governing the flooding phenomenon has not yet been established and few experimental data are currently available on flooding in nearly horizontal pipes. In particular, there exist large uncertainties in predicting initiation of flooding when pipes are slightly deviated from the horizontal or vertical position. In such a specific range, no theoretical or experimental studies have been attempted up to now. It is therefore the subject of this study to determine the limit of the stratified countercurrent flow (CCF), experimentally, to answer the question of how this flow limit is physically provoked, and to supplement the information to flooding phenomenon in a horizontal pipe slightly inclined from the horizontal plane.

In the present work, attention is focused on the flooding mechanism in circular pipes slightly downwardly inclined at various angles from the horizontal plane ($0° < \theta < 1°$). Two mechanisms governing the flooding phenomenon in circular pipes slightly inclined from the horizontal plane are suggested. The present data are compared with other flooding data published by several investigators, and the comparison with the slug formation models developed by several investigators in cocurrent horizontal flow is performed to explain the local effects of the void fraction on the initiation of flooding.

2. EXPERIMENTAL WORKS

2.1. Apparatus and experimental procedure

A schematic diagram of the experimental apparatus is shown in figure 1. The experimental loop is designed to allow countercurrent flow of air and water. It consists of two identical vessels, a test section, an air supply line and a circulating water loop. Two identical vessels have a bore diameter of 384 mm and a height of 800 mm. They are connected by a nearly horizontal test section with a length of 2160 mm. Two vessels and a test section are fitted to a metal frame whose one end is pivoted, while the other end can be raised by a screw jack. Any precise downward inclination between 0 and 30° with respect to the water flow can be allowed by raising one end of the metal

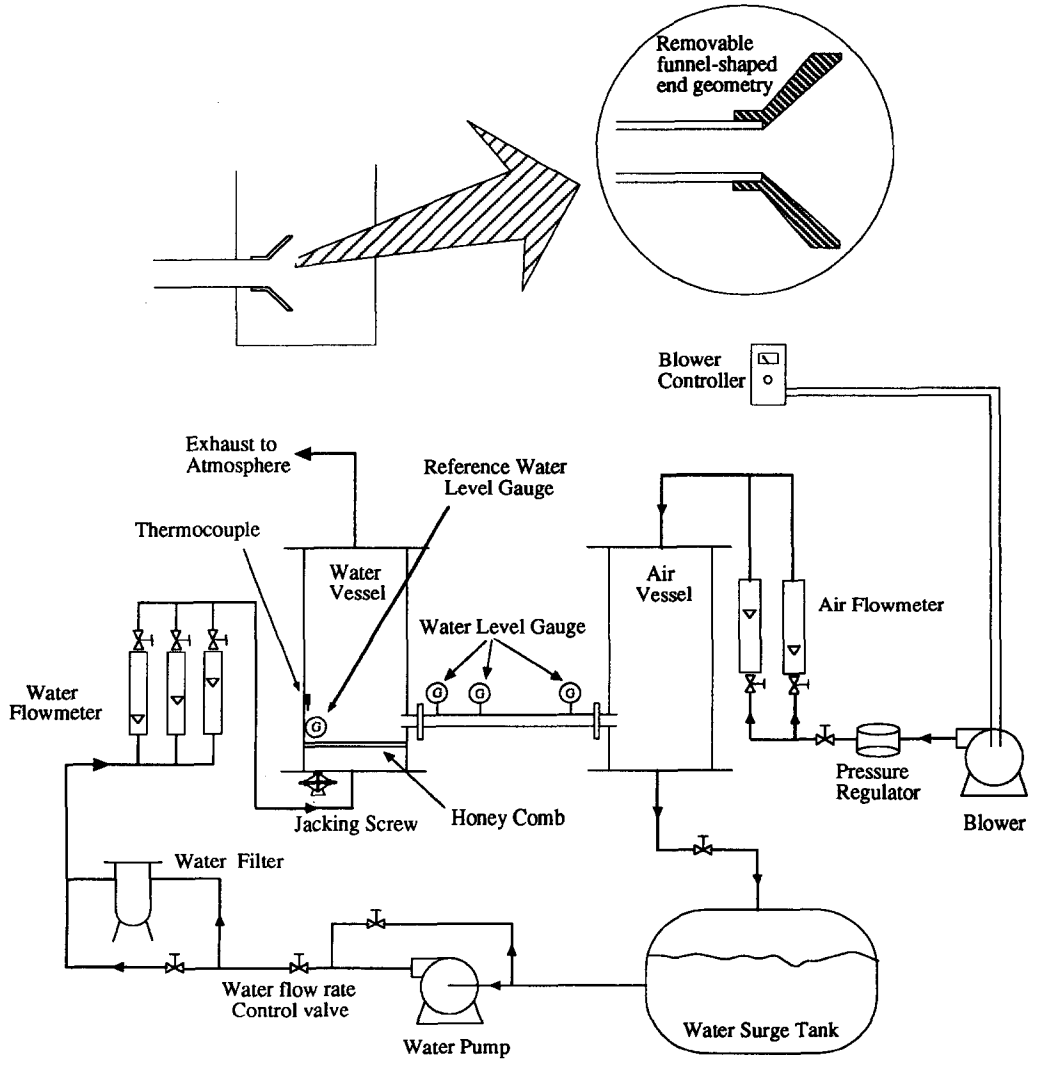

Figure 1. Experimental apparatus.

Table 1. Test section geometry and experimental conditions

Diameter (mm)	Entrance	Exit	Length (mm)	Inclination (degrees)	Water flow $j_L^{*1/2}$	Air flow (up to the onset of flooding)
70	sharp	sharp	2160	0.23–0.372	0.16–0.60	$j_G^{*1/2} \leqslant 0.45$
70	sharp	smooth	2160	0.23–0.372	0.15–0.56	$j_G^{*1/2} \leqslant 0.45$
70	smooth	sharp	2160	0.23–0.372	0.14–0.61	$j_G^{*1/2} \leqslant 0.46$
70	smooth	smooth	2160	0.23–0.372	0.14–0.63	$j_G^{*1/2} \leqslant 0.46$
70	sharp	sharp	2160	0.23	0.16–0.56	$j_G^{*1/2} \leqslant 0.43$
70	sharp	sharp	2160	0.69	0.14–0.55	$j_G^{*1/2} \leqslant 0.51$
70	sharp	sharp	2160	0.92	0.15–0.54	$j_G^{*1/2} \leqslant 0.51$
60	sharp	sharp	2160	0.23	0.18–0.58	$j_G^{*1/2} \leqslant 0.39$
60	sharp	sharp	2160	0.69	0.18–0.57	$j_G^{*1/2} \leqslant 0.49$
60	sharp	sharp	2160	0.92	0.18–0.65	$j_G^{*1/2} \leqslant 0.51$
40	sharp	sharp	2160	0.69	0.29–0.51	$j_G^{*1/2} \leqslant 0.43$
40	sharp	sharp	2160	0.92	0.26–0.52	$j_G^{*1/2} \leqslant 0.47$

frame using a screw jack. The inclination angle can be calculated by measuring the raised height of the bottom left of the metal frame from the ground and the horizontal length of the metal frame. Several test sections with three different diameters (i.d. = 0.04, 0.06 and 0.07 m) and three different downward inclinations ($\theta = 0.23$, 0.69 and 0.92°) with respect to the water flow are used as a test section. Two forms of end geometry are employed at the entrance and exit of the test pipe: one is the sharp-edged pipe geometry and the other the smooth-edged pipe geometry which is constructed by the removable funnel-shaped accessory fitting, as shown in figure 1. Table 1 shows test section geometry and experimental conditions tested in this work.

Air is supplied from the roots-type blower of the Samwon Industrial Co. with an air operation range of 0–6000 lpm and an operation pressure of 760 mmHg, through the pressure regulator and air flowmeter to the top of the air vessel. The pressure regulator between the air flowmeter and the blower ensures unperturbated air flow. The metered air passes through the test section and is then discharged to the atmosphere at the top of the water vessel. The main control of the air flow rate is performed by adjusting the speed of the motor in the blower using the motor controller, and three sub-control valves, which are installed in each flowmeter and in the pressure regulator, are used to supply the metered air. Normally the air in the entire air supply line is assumed to be at 1 atm pressure for calculating its properties. Air flow rates are measured by two rotameters connected in parallel.

The water flow forms a closed loop that includes a water surge tank, a circulating pump, a filter, three water flowmeters, the test section and two vessels. Metered water through the filter is supplied to the bottom of the water vessel and is discharged from the base of the air vessel to the water surge tank in order to provide the countercurrent flow. The control of the water flow is performed not only by the main control valve installed at the discharge line of the water pump, but also three sub-control valves installed at the discharge line of the each water flowmeter. A uniform water flow can be supplied by means of a honeycomb-like assembly installed in the lower plenum of the water vessel. In the neighborhood of the water pump, the bypass loop was added to the water-circulating closed loop in order to suppress the temperature rise of water due to heating of the pump impeller. The water flow rate was measured by three rotameters with different ranges, which were connected in parallel.

The experimental procedure is as follows: first, the diameter of the pipe tested is set and the parallel wire probes to measure the film thickness are carefully calibrated. Then the inclination angle is set to a fixed value. After any other geometric conditions have been set, the water flow rate is set and the air flow rate is increased in small steps until flooding is initiated. The film thickness is measured concurrently with each step of the air flow rate until flooding occurs. The flooding threshold is defined as being that condition in which the water starts to be accumulated in its supply vessel due to the air flow restricting the water flow. The onset of flooding is mainly determined by visual observation: carefully checking the flow pattern and the continuous rise of the water level in the water vessel. That is to say, the point at which the water level in the water vessel starts to rise continuously is considered to be the flooding threshold. In this work, flooding thresholds are usually well defined and repeatable.

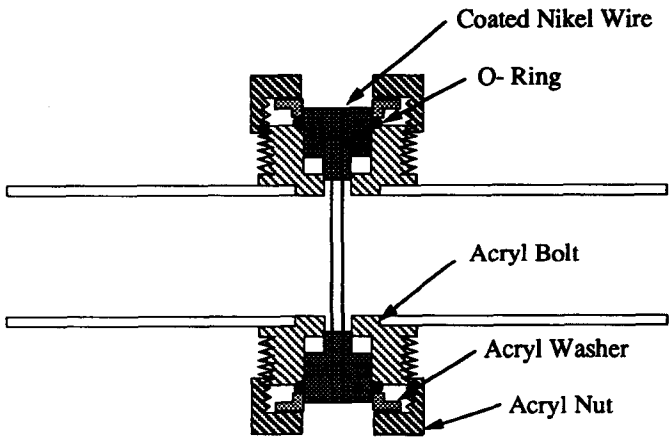

Figure 2. Schematic diagram of the water level gauge.

2.2. Water level measuring system and data acquisition system

In order to obtain the local void fraction or the water level within the test section, six parallel wire probes developed in this laboratory are attached to the test section along the vertical centerline of the pipe cross section. The detailed schematic diagram for the gauge is shown in figure 2. Also the water level between the installed water level gauges can be measured by scale marked rules attached at the outer surface of the test section. It is impossible to correct the possible variations in the water level across the width of the pipe. Thus the water level is assumed to be uniform across the width of the pipe. The electrical probes and the scale marked rules are employed together to measure the local void fraction. The electrodes consist of two coated nickel wires of 0.25 mm diameter, mounted vertically in the pipe 8 mm apart on the plane perpendicular to the direction of the flow. The wires are under slight tension and connected to the terminals at the top of the pipe. Six identical probes are located along the test section at 103, 230, 920, 1280, 1580 and 1880 mm from the water entrance, respectively.

In this work, three probes from the six are chosen after careful visual observation, and the chosen probes are used to measure the local void fraction. These gauges operate on the principle of the variation of the electrical resistance with changes in the water level between two vertically parallel electrodes. The variation of the resistance with the water level variation can be converted to the D.C. voltage drop signal across the two electrodes by the resistance circuit. To avoid distortion of the output signal due to polarization effects of the water. The A.C. carrier signal with a frequency of 10–20 kHz and amplitude of 0.5–0.8 V are applied to the terminal at the top of the pipe. The output voltage signal is amplified in the range 0.1–2.0 D.C.V. and transferred to the Hewlett–Packard Data Acquisition System. For accuracy, three probes were calibrated individually and then so many curves are employed as the calibration curves for these level gauges. Owing to the variation of conductivity or physical properties of water with the temperature variation of the water, one more reference gauge is designed to compensate for the drift and the distortion of the signal. The relative output signals are used as the final output signal and it is found that the response of these gauges is quite quadratic. For analog output voltage signals from the gauges, A/D conversion is performed at a sampling rate of 100 times per second. In this experiment, a total sampling time of 10.24 s is adopted, and data from the water level gauges are averaged over 10.24 s to evaluate the local time averaged void fractions. Using the HPIB interface, these sampled digital data are transferred to the HP3852A control unit, and recorded on a hard disk for later signal processing.

3. RESULTS AND DISCUSSION

3.1. Criticality for stratified two-phase flow

Gardner (1977) developed a theory of large lossless waves with two fluids in horizontal closed channels of arbitrary cross-section and derived the critical flow condition (i.e. the

condition for a stationary, infinitesimal interfacial wave) for stratified two-phase flow as follows:

$$\frac{j_L^{*2}}{(1-\epsilon)^3}+\frac{j_G^{*2}}{\epsilon^3}=\frac{\pi D}{4w}, \qquad [2]$$

where D is the inner pipe diameter and w is the width of the water surface. Equation [2] represents the conditions for the transition to super-critical flow where any small interfacial disturbance cannot propagate the flow. For an open channel flow (i.e. without the influence of gas flow) the above condition reduces to the accepted form of

$$\frac{j_L^{*2}}{(1-\epsilon)^3}=\frac{\pi D}{4w}. \qquad [3]$$

Therefore, we can define the Froude number determining the criticality of the stratified two-phase flow as follows:

$$\mathrm{Fr}=\frac{\dfrac{j_L^{*2}}{(1-\epsilon)^3}+\dfrac{j_G^{*2}}{\epsilon^3}}{\dfrac{\pi D}{4w}}. \qquad [4]$$

This definition for the Froude number was also used by Kukita *et al.* (1989) and Katayama *et al.* (1991).

We can determine from [4] whether the water flow condition at a certain location is sub- or super-critical, if the liquid flow rate, gas flow rate and void fraction at that location are measured. Visual observation showed that two distinct water levels existed in the pipe because the hydraulic jump was developed at a certain location of the pipe. This situation, in which two distinct water levels coexisted, occurred in the particular range of the experimental parameters. It is seen from the open channel flow theory that one corresponds to the super-critical state, and the other to the sub-critical state. The detailed observations are presented in the next section. Two distinct water levels (or void fractions) were measured at two locations where the water depth was highest to determine the local criticality of the water flow. On the other hand, when the hydraulic jump was not observed in the pipe until flooding occurred, only one highest water level was measured. Results are shown in figure 3 with [2]. It is found from figure 3 that water levels or void fractions measured

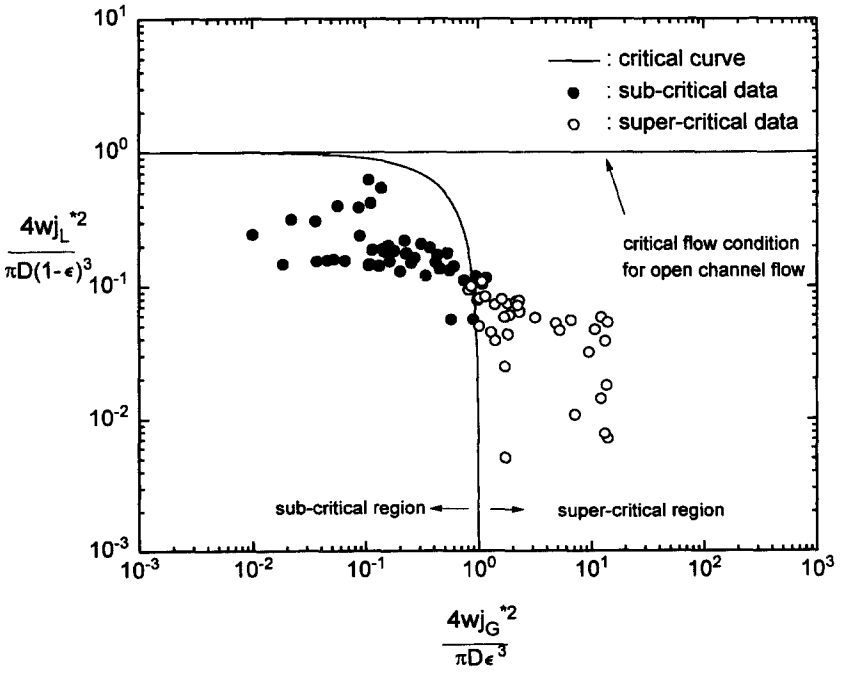

Figure 3. Criticality of the stratified two-phase flow.

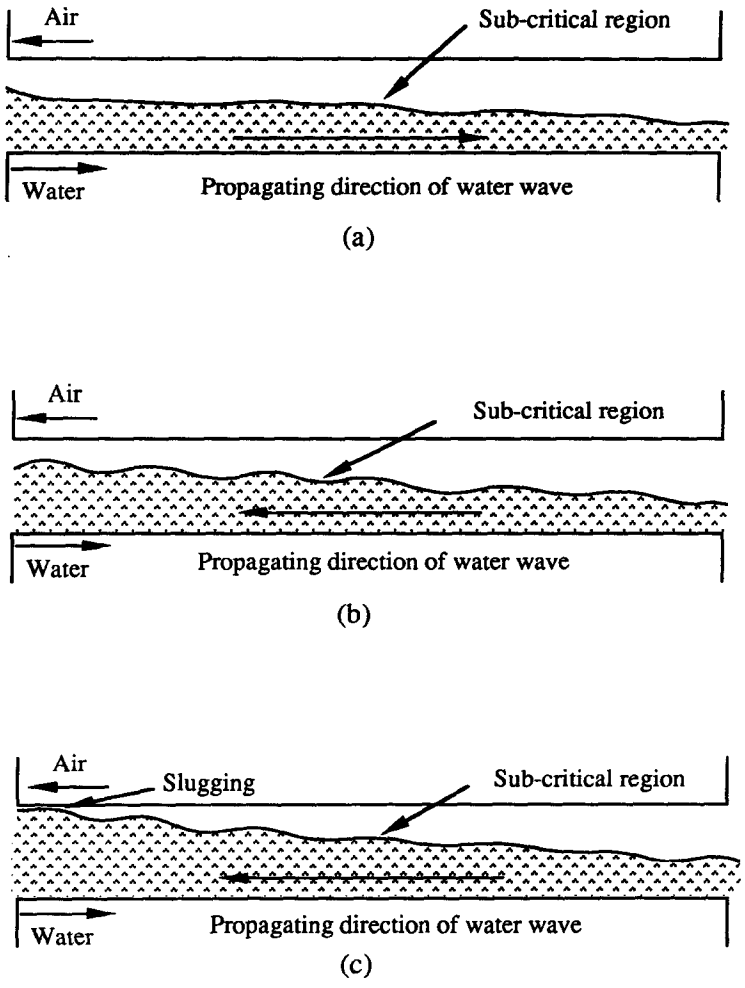

Figure 4. Flow patterns at the inclination angle of 0.23°.

simultaneously in two regions are well divided into two regions: sub- and super-critical region. As a result, it is found that two distinct water levels measured simultaneously correspond to sub- and super-critical flow, respectively.

3.2. Visual observations

Depending on the water flow rates and inclination angles, initiation of flooding can be observed to take place differently. At the lowest inclination angle ($\theta = 0.23°$), the observed flow patterns are sequentially given in figure 4(a), (b) and (c). As shown in figure 4(a), there exists a water level gradient decreasing toward the exit of the water flow. As the air flow rate increases, the water level gradient becomes steeper as shown in figure 4(b). It is observed that the initial direction of the propagation of the water waves is changed from the same direction of the water flow to that of the air flow even though little air flow is supplied. Therefore, the water waves grow, propagating toward the entrance of the water flow. As a result, the water waves provide the narrowest restriction to the air passage at the water entrance where flooding is initiated. It is noted that flooding is initiated by the sudden growth of a wave around the entrance of the water flow at all times as shown in figure 4(c). The transition to flooding occurs very rapidly with a small increase of the air flow rate after the formation of a water slug near the water entrance, and thus it is hard to distinguish between the point of the slug formation and the flooding threshold.

At higher inclination angles ($\theta = 0.69°$), the observed flow patterns are sequentially given in figure 5(a), (b) and (c). The initial flow pattern is similar to that of figure 4(a) except for more gentle water

level gradients. A peculiar observation shows that a hydraulic jump is created in the pipe if the air flow rate increases up to a critical value for a given inclination as shown in figure 5(b). It is a well-known fact from the open channel flow theory that if there exist two distinct water levels at a given water flow rate, one corresponds to the sub-critical flow and the other to the super-critical flow. As can be seen in figure 5(b), a further increase in air flow rate pushes the location of the hydraulic jump toward the entrance of the water flow, and makes water waves in the sub-critical region propagate in the opposite direction to the initial water flow. These waves, traveling in the same direction as the air flow, gradually grow downstream of the hydraulic jump until the onset of slugging occurs. Transition to flooding always occurs a little downstream of the hydraulic jump due to the onset of slugging. The onset of flooding is observed to be consistent with the onset of slugging.

At the highest inclination angle ($\theta = 0.92°$) and a high water flow rate ($j_L^{*1/2} \geqslant 0.4$), the observed flow patterns are greatly different from the above two cases and are sequentially given in figure 6(a), (b) and (c). As seen in figure 6(a), the initial flow pattern is almost similar to that of figure 5(a). However, only the super-critical region exists throughout the pipe and no hydraulic jump occurs within the pipe until flooding occurs. The direction of the propagation of the water waves is always the same as that of the initial water flow. The initial water level in the entrance tank is always maintained below the top of the pipe to avoid the water flow being choked at the pipe entrance. Because of the large water level difference between the water vessel and the pipe, the major portion of the air momentum is concentrated on the steepest region instead of the water wave in

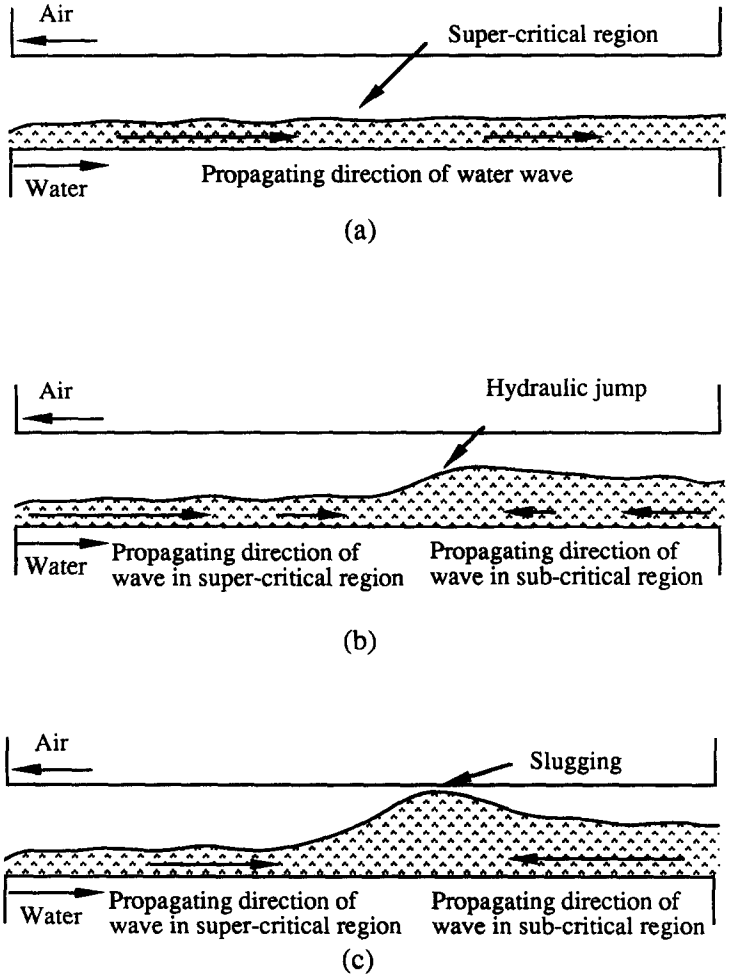

Figure 5. Flow patterns at the inclination angle of 0.69°.

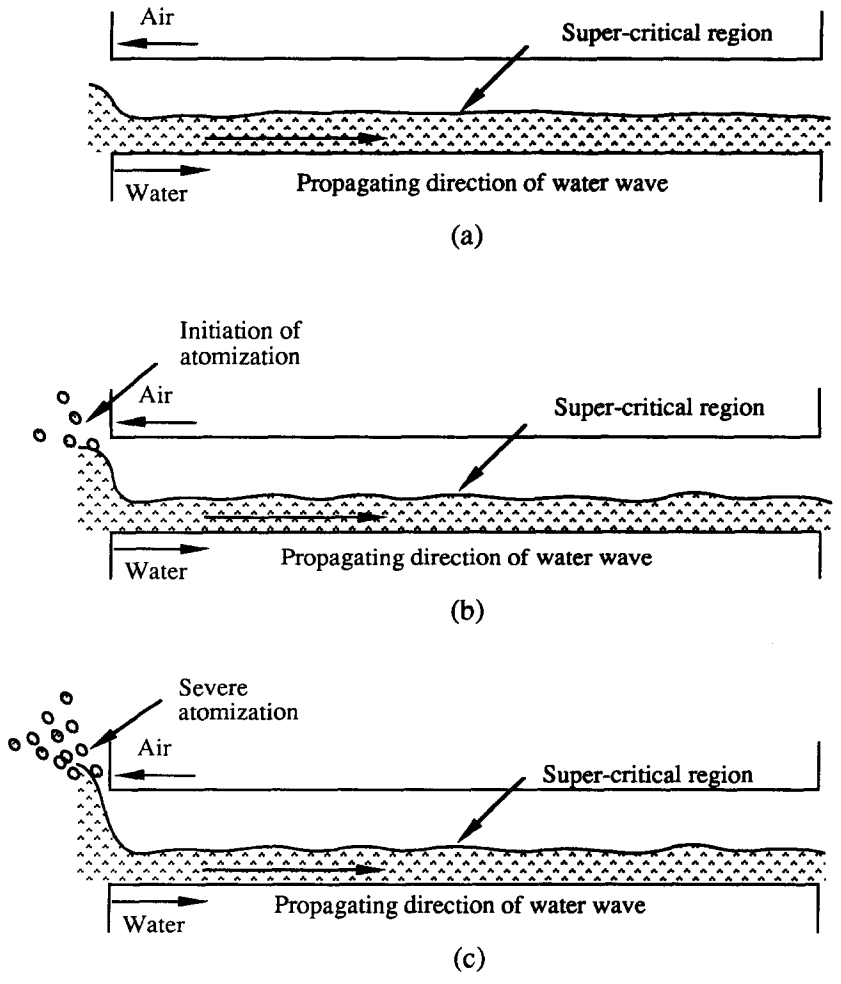

Figure 6. Flow patterns at the inclination angle of 0.92° and higher water flow rate.

the super-critical region. Therefore, a little increase in the air flow near the onset of flooding results in breaking the edge of the steepest region, i.e. atomization as shown in figure 6(b). The water level in the water supply tank is observed to continue to rise above a certain air flow rate. This condition corresponds to the definition of flooding threshold. As time goes by, the water level in the water supply tank becomes higher than the top of the pipe, and then the water flow is abruptly choked at the entrance of the pipe as shown in figure 6(c). Until flooding occurs, it is observed that no slug formation occurs and flooding is always initiated at the entrance of the water flow due to atomization.

3.3. Flooding mechanisms

Based on the visual observations, it is suggested that the flooding phenomenon in nearly horizontal pipes is govern by two mechanisms: the "inner flooding" and "entrance flooding". "Inner flooding" includes a hydraulic jump-induced flooding which has also been observed by other investigators, Siddiqui *et al.* (1986) and Kawaji *et al.* (1991). Flooding is initiated by the sudden growth of waves which already exist in the pipe before the onset of flooding. The waves created by the air shear force continue to grow until flooding occurs, propagating toward the entrance of the water flow. If the length of the pipe is short, the waves cannot grow enough to initiate flooding. That is, whether flooding is initiated or not is governed by the past experiences of the waves. Flow patterns corresponding to the "inner flooding" mechanism are shown in figures 4 and 5. As shown in both figures, flooding is initiated in the sub-critical region by sudden wave growth when the air

flow increases up to a threshold value. The location of the onset of flooding varies from the entrance to the exit of the water flow, with the water flow rate and the inclination angle. The transition criterion corresponding to the onset of flooding is approximately consistent with that of the slug formation, although the random appearance of the solitary waves is observed prior to flooding for the relatively thin water film. Initially, water waves propagate in the same direction as that of the water flow. However, the stationary waves are created prior to flooding and a little increase in the air flow rates makes these waves propagate in the opposite direction of the initial water flow. Until wave instability occurs, these waves moving in the opposite direction of the water flow gradually grow. At the lowest inclination angle ($\theta \leqslant 0.23°$), a hydraulic jump is not observed. Therefore, it should be distinguished from hydraulic jump-induced flooding. However, flooding is observed to take place by the same mechanism, wave instability. Thus it is reasonable that the data obtained in this range should be included in the mechanism of "inner flooding".

On the other hand, at inclination angles higher than 0.69° and high water flow rates ($j_L^{*1/2} \geqslant 0.4$), "entrance flooding" is the dominant mechanism of the onset of flooding. Flooding is not governed by the historical phenomenon but by the local phenomenon as shown in figure 6(a), (b) and (c). The past experience of the waves have little effect on the initiation of flooding. Initiation of flooding is only governed by the entrance geometry of the water flow, i.e. local condition. The flow condition is maintained as the super-critical state until flooding occurs. Therefore the water waves cannot propagate to the upstream. Flooding is always observed to be initiated at the entrance of the water flow. It is a noteworthy observation that flooding is always provoked without slugging. The onset of flooding in a nearly horizontal pipe is independent of the onset of the slugging condition within this range. Quantitative study on "entrance flooding" was not performed in this work. So a definite criterion by which "inner flooding" and "entrance flooding" can be distinguished is not yet clear. As the water flow is injected into the pipe only by the head difference, the water flow rate tested is restricted to within the narrow limits in this work. Therefore, only a few data can be obtained for higher water flow rates. However, it is found that initiation of flooding greatly depends on the method of introducing the water into the pipe for the high inclinations and water flow rates.

3.4. *Effect of pipe diameter*

Several experiments were performed in which the diameter of the test section was varied to examine the effect of pipe diameter. Results are displayed in figure 7 in terms of $j_K^{*1/2}$ parameters

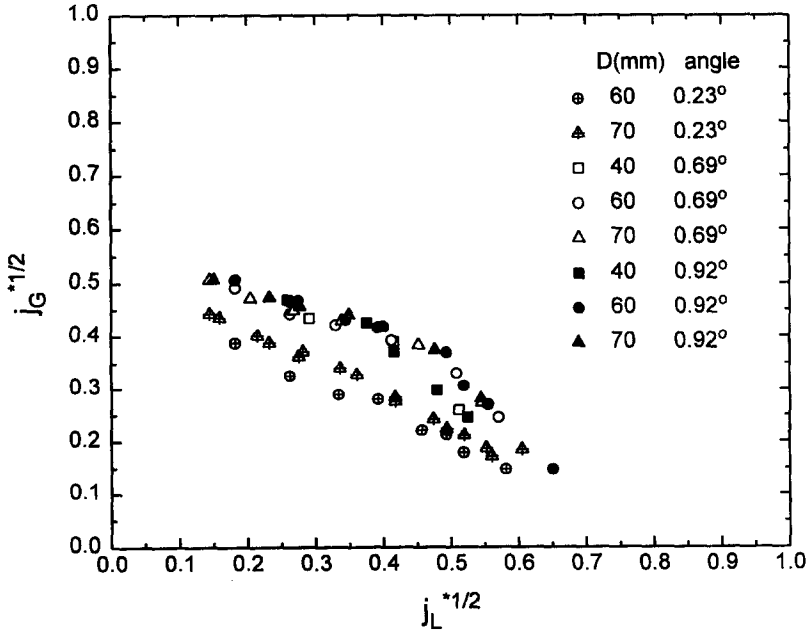

Figure 7. Effect of pipe diameter on flooding.

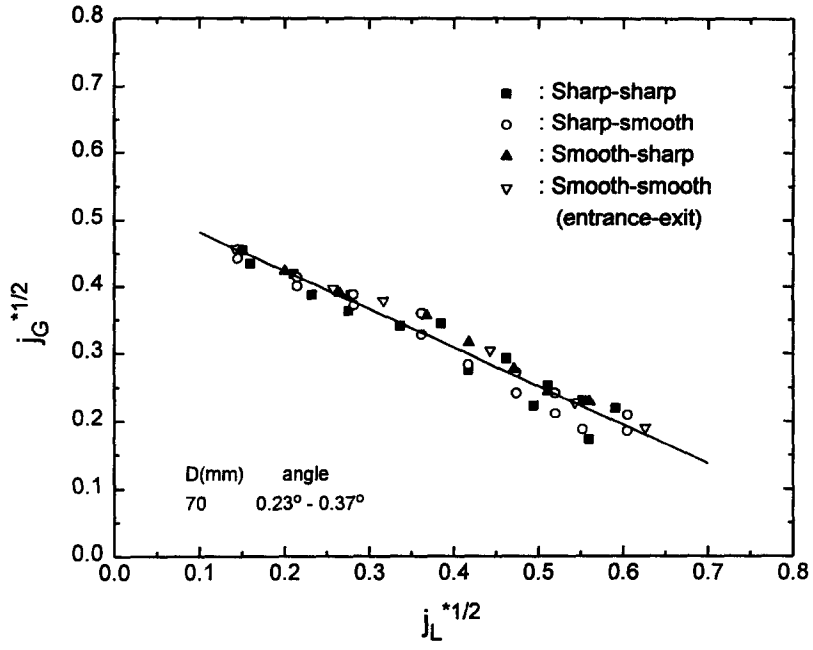

Figure 8. Effect of pipe end geometry on flooding.

defined by $j_K^* = j_K/\sqrt{gD(\rho_L - \rho_G)/\rho_K}$, where j_K and ρ_K are the superficial velocities and densities of phase K(K = L for the liquid phase and K = G for the gas phase), D is the diameter of the pipe and g is the gravitational acceleration. Up to now, $j_L^{*1/2}$ and $j_G^{*1/2}$ have been a convenient way of displaying the flooding data. So in this work, $j_K^{*1/2}$ parameters are also used to display flooding data and to compare flooding data with those of other investigators. At higher water flow rates ($j_L^{*1/2} \geqslant 0.4$), the data have steeper slopes than the data at lower water flow rates and flooding is mainly initiated from the mechanism of "entrance flooding". The quantitative criterion from which the mechanism of "entrance flooding" becomes predominant is not clear. As evident from figure 7, it is difficult to find the effect of pipe diameter on "inner flooding" at the same angle. It is interesting that the variation of the diameter has a negligible effect on "inner flooding" for the 40–70 mm range. However, the effect of pipe diameter on flooding due to "entrance flooding" is not clear.

3.5. Effect of pipe end geometry

Tests for four kinds of pipe end geometry combinations are performed. Funnel-shaped end geometry is designated as "smooth" and inherent pipe end geometry is named "sharp" for convenience. The removable funnel-shaped accessory fitting can easily be attached or removed. Flooding data due to "inner flooding" are collected in order to investigate the effect of pipe end geometry. As shown in figure 8, $j_G^{*1/2}$ is almost the same at the same $j_L^{*1/2}$ for the different pipe end geometry combinations. Therefore it is found that the criterion for transition to flooding in a nearly horizontal stratified flow is independent of the pipe end geometry within the range tested.

3.6. Effect of inclination angle

The inclination angle has a great effect on the location where flooding occurs and the flow pattern just prior to the onset of flooding. It is observed that a hydraulic jump never occurs and flooding is always initiated at the entrance section of the water flow in the case of the angle of 0.23°. However, for other angles (0.69 and 0.92°), a hydraulic jump is developed at some point along the pipe and flooding is initiated a little downstream of the hydraulic jump. That is to say, the location where flooding occurs moves continuously from the entrance to the exit of the water flow as the inclination angle increases. If the water flow rate is large enough at this time, the location where flooding occurs is suddenly switched from the exit to the entrance of the water flow. For high water

flow rates, a liquid hump with high liquid level is developed at the entrance section of the water flow, causing a narrow air passage. So, most of the air shear momentum is concentrated on this hump. As a result, a sudden transition of the location where flooding occurs takes place. Therefore, entrance geometry plays an important role in the flooding phenomenon only for high water flow rates.

As shown in figure 9, the data for the lowest angle, 0.23°, have a considerably lower value of $j_G^{*1/2}$ than those for the other angles. On the other hand, the data for an angle of 0.92°, are slightly higher than those for an angle of 0.69°. It is a noticeable surprise that there is considerable deviation of data within quite a narrow range of inclination ($0° < \theta < 1°$). In particular, for the low water flow rates ($j_L^{*1/2} < 0.4$) the deviation is more severe. It is found that flooding is very sensitive to the inclination angle for a very slightly inclined horizontal pipe. As the inclination angle is increased, a higher air flow rate is needed to initiate flooding as seen in figure 9. This observation that a higher air flow rate is required to provoke flooding as the inclination angle becomes steeper is consistent with that by Barnea *et al.* (1986). They found that the effect of inclination was not monotonic and that the flooding gas velocity at a given liquid velocity increased and then decreased as the inclination angle increases from horizontal to vertical. Also Kawaji *et al.* (1991) inferred that the highest flooding curve might lie between 22.5 and 45°. So it is reasonable that the flooding curve becomes higher as the inclination becomes steeper within the range of our work. The data obtained are plotted together with those by Barnea *et al.* (1986) who investigated the inception of flooding in inclined pipes in the whole range of inclinations. It is seen from figure 9 that our results underpredict the flooding criterion compared to the data of Barnea *et al.* (1986). Flooding data for the inclination angle of 0.92° are slightly lower than those of Barnea *et al.* (1986) for the inclination angle of 1° at low water rates ($j_L^{*1/2} < 0.4$) and slightly higher than those at high water flow rates ($j_L^{*1/2} > 0.4$).

Barnea *et al.* (1986) reported that at low liquid and high gas flow rates the hump around the porous entrance section was very small and flooding was initiated due to interfacial instability at a certain location along the pipe. This observation is fairly well consistent with the present one. Note that the porous entrance is usually considered to be a smooth entrance that should be free of local disturbances. Using the porous entrance section allows injection of the liquid with a low axial velocity. As a result, a slightly higher gas velocity is needed to initiate flooding at low liquid flow rates. However, at high liquid and low air flow rates the situation is reversed. At moderate

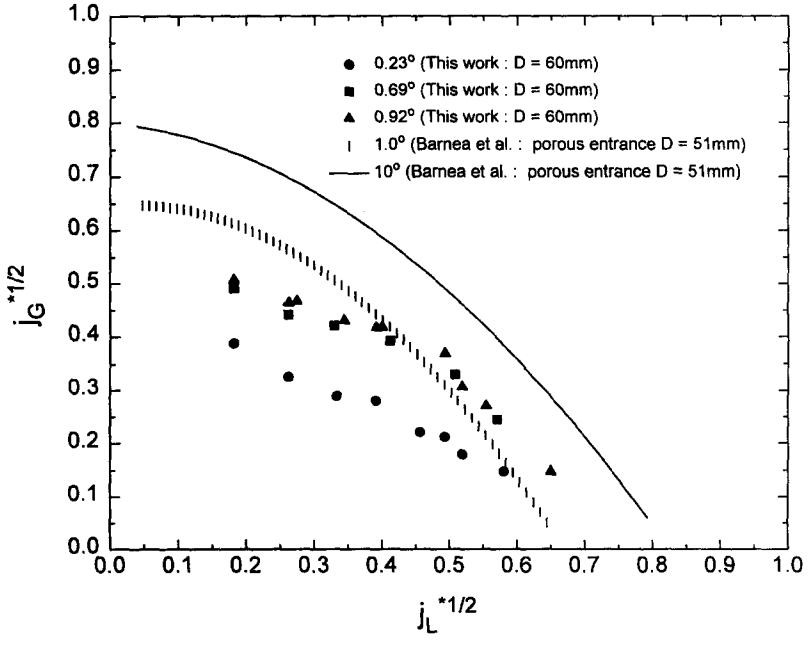

Figure 9. Effect of inclination angle on flooding.

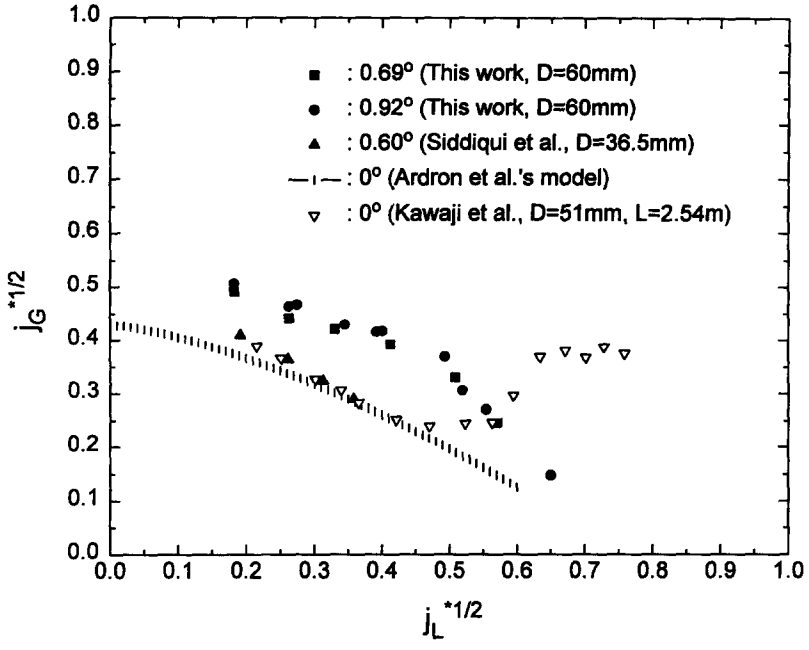

Figure 10. Comparison of the present data with other flooding data.

and high liquid flow rates, Barnea *et al.* (1986) found that initiation of flooding using the porous entrance section was a local phenomenon generated at the entrance section itself as a result of a locally high liquid level built at the entrance. Although the liquid is introduced through a porous wall, due to the inclination and the mixing section, the injection of the high liquid flow generates a locally high liquid level. This entrance condition provides a narrow restriction to the gas passage. However, this initial disturbance at the entrance was not severe in our experiments. As a result, somewhat lower gas flow rates are required to initiate flooding when the liquid is introduced through the porous section, especially at high water flow rates.

3.7. Comparisons of the present data with other flooding data

Figure 10 compares the present data with the predictions of Ardron *et al.*'s (1986) model for a vertical-to-horizontal pipe ($\theta = 0°$) and those of Siddiqui *et al.* (1986) for a vertical-to-downwardly inclined pipe ($\theta = 0.6°$) and those of Kawaji *et al.* (1991) for a vertical-to-horizontal pipe ($\theta = 0°$). Ardron *et al.*'s (1986) model is based on hydraulic jump-induced flooding near the elbow and the data of Siddiqui *et al.* (1986) are also consequences of hydraulic jump-induced flooding. The data set of Kawaji *et al.* (1991) includes data as a result of hydraulic jump-induced flooding. Thus, the data corresponding to the hydraulic jump-induced flooding mechanism are collected and plotted in figure 10. The calculations for Ardron *et al.*'s (1986) model are performed for an air–water flow in a tube with $D = 60$ mm and $L = 2160$ mm, of which the geometric conditions are the same as those of the present work.

It is evident from figure 10 that the present data show higher air flow rates than those of Siddiqui *et al.* (1986) and the predictions of Ardron *et al.*'s model (1986). Siddiqui *et al.* (1986) found that the hydraulic jump was always generated near an elbow and flooding occurred downstream of the hydraulic jump. That is to say, the hydraulic jump produces initial unstable flow disturbances even if there is no air flow for their experiments with a vertical section. However, as there is no vertical section in our work, the hydraulic work is not created if there is no air flow. A hydraulic jump is generated at a certain location along the pipe when there is a sufficient air flow rate. Kawaji *et al.* (1991) also found that addition of an elbow and a vertical section to an inclined pipe results in greater disturbances in the entrance region of the inclined pipe, just downstream of the elbow, due to a flow pattern transition from annular to stratified flow. Therefore, it is not surprising that the present data, with no vertical section, show higher air flow rates than those of Siddiqui *et al.* (1986) and those of Ardron *et al.* (1986).

The flooding curve of Kawaji *et al.* (1991) shows a similar trend to that of Siddiqui *et al.* (1986) at low water flow rates ($j_L^{*1/2} \leqslant 0.4$), because their test section also consists of a vertical part. Here, other data for vertical-to-inclined pipes are excluded because the flooding mechanism is not hydraulic jump-induced flooding in those cases. Whereas, a severe deviation exists at high water flow rates ($j_L^{*1/2} \geqslant 0.4$). Kawaji *et al.* (1991) reported that at moderate water flow rates ($0.4 \leqslant j_L^{*1/2} \leqslant 0.7$), the flooding mechanism changed to slugging at the exit and at high liquid flow rates ($j_L^{*1/2} \geqslant 0.8$), flooding occurred in the vertical section near the porous liquid entrance section rather than in the horizontal section. So the severe deviation between our data and those of Kawaji *et al.* (1991) is due to the different flooding mechanism at the moderate and high liquid flow rates ($j_L^{*1/2} \geqslant 0.4$).

3.8. Comparisons with slug formation models

In the case of "inner flooding", the formation of a water slug was observed at the inner location of the pipe just before the onset of flooding. The transition criterion for the onset of flooding was observed to be consistent with that for slug formation. Therefore, it is interesting to compare the present data with the slug formation models proposed by several investigators. On the other hand, no slug formation was observed to take place in the case of "entrance flooding".

Most slug formation models were expressed in terms of the void fraction and the non-dimensional air superficial velocity. Taitel & Dukler (1976) analyzed the force acting on a solitary wave in a duct and derived an expression, which could be approximated by the following dimensionless equation for a tube:

$$j_G^* = \epsilon^{5/2}. \qquad [5]$$

In their derivation, they used the equilibrium void fraction. Mishima & Ishii (1980) extended the finite amplitude wave analysis of Kordyban & Ranov (1970) and incorporated the concept of the most dangerous wave to derive the following dimensionless equation:

$$j_G^* = 0.487\epsilon^{3/2}. \qquad [6]$$

Mishima & Ishii (1980) also used the equilibrium void fraction. This expression is almost identical to the empirical correlation of Wallis & Dobson (1973) who conducted air–water slugging experiments with stationary liquid,

$$j_G^* = 0.5\epsilon^{3/2}. \qquad [7]$$

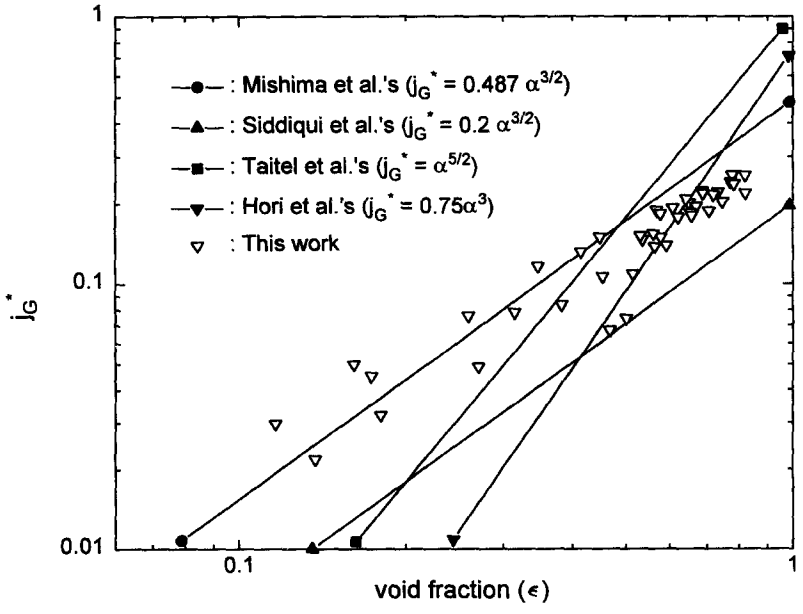

Figure 11. Local void fraction in sub-critical region vs j_G^*.

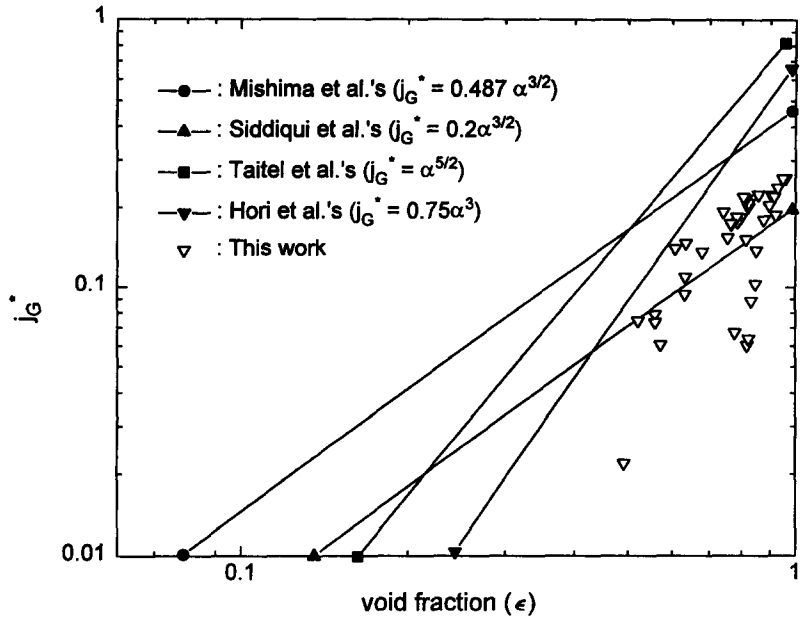

Figure 12. Local void fraction in super-critical region vs j_G^*.

Siddiqui *et al.* (1986) obtained the empirical correlation from their experimental data as seen in [1], in which the local void fraction at the crest of the hydraulic jump was used. Hori *et al.* (1985) conducted an experiment for slugging in a 200 mm diameter pipe and obtained the following empirical correlation:

$$j_G^* = 0.75\epsilon^3. \qquad [8]$$

As can be seen in [1], [5], [6], [7] and [8], the exponents of the void fraction term of the published models and the correlations vary from 3/2 to 3 and the definitions of the void fraction are different from one another. In one case, the equilibrium void fraction was used, in another case, the local void fraction at the crest of the wave was used. Up to now, it is not clear why the exponent of the void fraction term of the slug formation model varies. It is thus necessary to carefully define and use the void fraction in the process of developing the slug formation model.

The measurements of the void fractions in two regions, i.e. the sub- and super-critical regions, were performed just prior to the onset of flooding in order to examine the effect of the local void fraction on the slug formation model. The water levels in both regions were not uniform because of a hydraulic gradient. Therefore, the measurements for the void fractions in both regions were carried out at the location at which the water level was the highest.

Results are plotted in figures 11 and 12 in terms of the local void fraction and the non-dimensional air superficial velocity. As shown in figures 11 and 12, when the void fraction measured in the sub-critical region is used in the slug formation model, Mishima & Ishii's (1980) model well predicts the trend of the present data without systematic errors, though some deviations exist with the inclination angles. On the other hand, when the void fraction measured in the super-critical region is used, the prediction of Mishima & Ishii's (1980) model shows a great deviation from the present data, but Taitel & Dukler's (1976) model better predicts the present data than Mishima & Ishii's (1980) model. It is interesting that the use of void fraction in the different regions (i.e. sub- or super-critical region) results in the different dependence of the non-dimensional superficial air velocity on void fraction. It is thus inferred that the difference in the exponent of the void fraction term in both models is attributed to the void fraction which is used.

Siddiqui *et al.* (1986) observed hydraulic jump-induced flooding in vertical-to-horizontal pipes and developed the empirical correlation as [1]. This hydraulic jump-induced flooding was observed in the present work. It is thus interesting if the present data, which correspond to the hydraulic jump-induced flooding, are compared with that of Siddiqui *et al.* (1986). The hydraulic jump-induced flooding was not always observed to take place with the given experimental conditions.

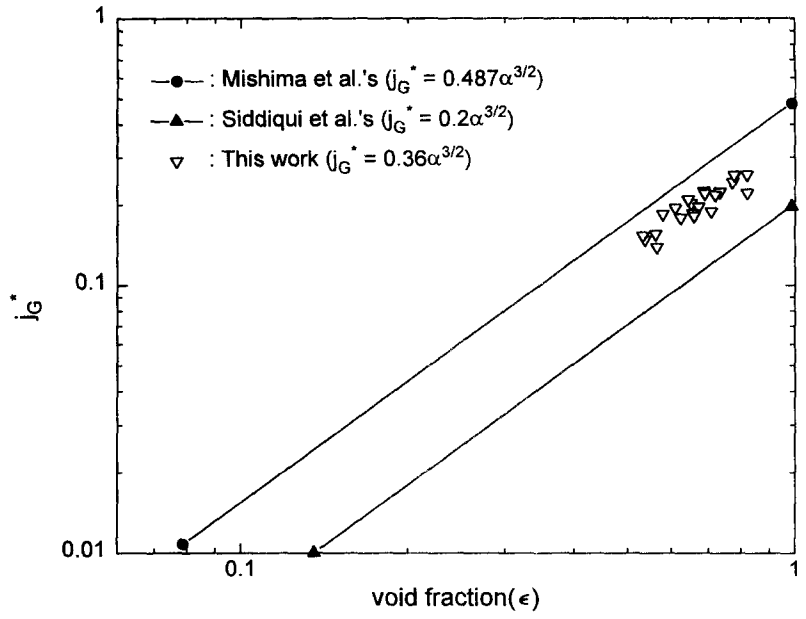

Figure 13. Comparison with other hydraulic jump-induced flooding data.

For an inclination angle lower than 0.23°, flooding was not initiated due to the hydraulic jump-induced flooding. The present flooding data which are due to the hydraulic jump-induced flooding are correlated as follows:

$$j_G^* = 0.36\epsilon^{3/2}, \qquad [9]$$

where the void fraction in the sub-critical region is used. Results are shown in figure 13. As can be seen in figure 13, the trend of this work is consistent with that of Siddiqui *et al.* (1986) except that a little higher air flow rates are required to initiate slugging in our results. The difference may be attributed to the difference in the geometry of the test section. The test section of Siddiqui *et al.* (1986) was composed of a vertical section and an inclined section. Therefore, the water flow

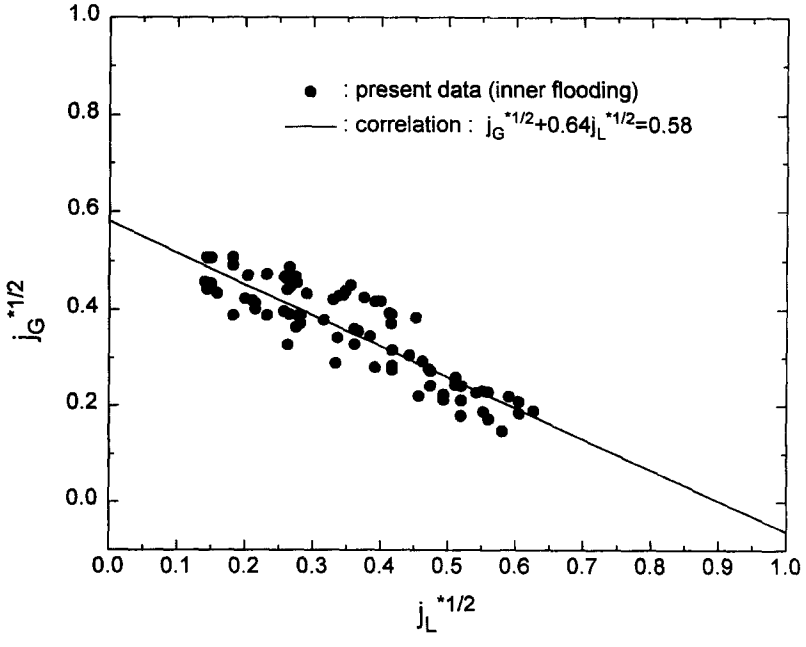

Figure 14. Inner flooding correlation.

near the elbow becomes more unstable than in our case because a flow pattern transition from annular to stratified flow takes place near the elbow. Such an unstable flow condition near the elbow requires lower air flow rates to provoke flooding.

3.9. Development of flooding correlation

A flooding correlation corresponding to "inner flooding" was developed. Correlation development for "entrance flooding" was not carried out because very limited data were obtained for the case of "entrance flooding". Figure 14 shows the air flow rates at which inner flooding occurs for a range of water flow rates. As the range of the inclination angle is limited to within a narrow range, the correlation was developed in terms of Wallis parameters as follows:

$$j_G^{*1/2} + 0.64 j_L^{*1/2} = 0.58. \quad [10]$$

4. CONCLUSIONS

On the basis of the experimental studies, the following conclusions are obtained: the mechanisms of the onset of flooding can be categorized into two groups, i.e. "inner flooding" and "entrance flooding". In the case of "inner flooding", flooding is initiated by sudden wave growth, and the criterion for the onset of flooding is approximately consistent with that of slug formation. In the case of "entrance flooding", no slug formation occurs. Flooding by "inner flooding" is not affected by the pipe end geometry. Flooding by "inner flooding" occurs at the inner location of the test section and in the sub-critical region. The effect of the pipe diameter on flooding due to "inner flooding" is negligible for the 40–70 mm range and the effect on "entrance flooding" remains a subject for further examination. The transition criterion for the onset of flooding is very sensitive to the inclination angle. A slight increase in the inclination angle has a great effect on the location where flooding occurs and on the flow patterns. Therefore, it is one of the important parameters governing flooding in nearly horizontal pipes. Void fractions in the two regions are measured: void fractions in the sub-critical region and in the super-critical region. When the void fraction in the sub-critical region is selected as a parameter for the flooding correlation. Mishima & Ishii's (1980) model well predicts the present data. On the other hand, if the void fraction in the super-critical region is selected. Taitel & Dukler's (1976) model better fits the data. The variation in the exponents of the void fraction terms in the slug formation models is attributed to the void fraction which is used as the parameter for the flooding correlation.

REFERENCES

ARDRON, K. H. & BANERJEE, S. 1986 Flooding in an elbow between a vertical and a horizontal or near-horizontal pipe. Part II: theory. *Int. J. Multiphase Flow* **12,** 543–558.

BARNEA, D., BEN YOSEPH, N. & TAITEL, Y. 1986 Flooding in inclined pipes-effect of entrance section. *Can. J. Chem. Engng* **64,** 177–184.

GARDNER, G. C. 1977 Motion of miscible and immiscible fluids in closed horizontal and vertical ducts. *Int. J. Multiphase Flow* **3,** 305–318.

GARDNER, G. C. 1979 Onset of slugging in horizontal ducts. *Int. J. Multiphase Flow* **5,** 201–209.

HORI, K., UENO, T. & KAWANISHI, K. 1985 Gas–liquid two-phase flow in large diameter tube (II. Horizontal concurrent flow). *Proc. of 22nd Japan National Heat Trans. Symp.*, p. 356.

KATAYAMA, J., NAKAMURA, H. & KUKITA, Y. 1991 Flow regime transition in stratified two-phase flow including a hydraulic jump. *Proc. of Int. Conf. on Multiphase Flow*, Tsukuba, pp. 7–10.

KAWAJI, M., THOMPSON, L. A. & KRISNAN, V. S. 1991 Countercurrent flooding in vertical-to-inclined pipes. *Exp. Heat Transfer* **4,** 95–110.

KORDYBAN, E. S. & RANOV, T. 1970 Mechanism of slug formation in horizontal two-phase flow. *ASME J. Basic Engng* **92,** 857–864.

KUKITA, Y., NAKAMURA, H., ANODA, Y. & TASAKA, K. 1989 Hot leg characteristics during two-phase natural circulation in pressurized water reactor. *Proc. of 4th Int. Conf. on Nuclear Reactor Thermal Hydraulics*, Karlsruhe, pp. 465–470.

LEE, S. C. & BANKOFF, S. G. 1983a A critical review of the flooding literature. In *Multiphase Science and Technology* (Edited by HEWITT, G. F., DELHAYE, J. M. & ZUBER, N.), Vol. 2, pp. 95–180. Hemisphere, Washington, D.C.

LEE, S. C. & BANKOFF, S. G. 1983b Stability of stream–water countercurrent flow in an inclined channel: flooding. *ASME J. Heat Transfer* **105,** 713–718.

MISHIMA, K. & ISHII, M. 1980 Theoretical prediction of onset of horizontal slug flow. *ASME J. Fluids Engng* **102,** 441–445.

SIDDIQUI, H., BANERJEE, S. & ARDRON, K. H. 1986 Flooding in an elbow between a vertical and a horizontal or near-horizontal pipe. Part I: experiments. *Int. J. Multiphase Flow* **12,** 531–541.

TAITEL, Y. & DUKLER, A. E. 1976 A model for predicting flow regime transition in horizontal and near horizontal gas–liquid flow. *AIChE Jl* **22,** 47–55.

WALLIS, G. B. & DOBSON, J. E. 1973 The onset of slugging in horizontal stratified air–water flow. *Int. J. Multiphase Flow* **1,** 173–193.